

Joint Beamforming Design for RIS-enabled Integrated Positioning and Communication in Millimeter Wave Systems

Junchang Sun, Shuai Ma, and Shiyin Li

Abstract

Integrated positioning and communication (IPAC) system and reconfigurable intelligent surface (RIS) are both considered to be key technologies for future wireless networks. Therefore, in this paper, we propose a RIS-enabled IPAC scheme with the millimeter wave system. First, we derive the explicit expressions of the time-of-arrival (ToA)-based Cramér-Rao bound (CRB) and positioning error bound (PEB) for the RIS-aided system as the positioning metrics. Then, we formulate the IPAC system by jointly optimizing active beamforming in the base station (BS) and passive beamforming in the RIS to minimize the transmit power, while satisfying the communication data rate and PEB constraints. Finally, we propose an efficient two-stage algorithm to solve the optimization problem based on a series of methods such as the exhaustive search and semidefinite relaxation (SDR). Simulation results show that by changing various critical system parameters, the proposed RIS-enabled IPAC system can cater to both reliable data rates and high-precision positioning in different transmission environments.

Index Terms

Integrated positioning and communication, reconfigurable intelligent surface, millimeter wave, joint beamforming optimization.

I. INTRODUCTION

A. Backgrounds and Motivations

Integrated sensing and communication (ISAC) is regarded as an important and promising technology for future beyond 5G (B5G) and 6G wireless networks [1], [2]. The ISAC system aims to achieve high-quality communication services and powerful sensing capabilities at the same time. Commonly, the radar is applied to the system to enable the sensing function, such as

joint radar and communication (JRC) [3] and joint communication and radar (JCR) [4]. Recently, the widespread application of the millimeter waves enables us to consider the advantages of using this technology to design the integrated system.

In the case of the millimeter wave assisted integrated system, we are more concerned with the positioning performance in sensing capabilities. Relay on high bandwidth and high temporal resolution, millimeter waves have potentials for both communication and positioning. Therefore, we formulate an integrated positioning and communication (IPAC) system with the millimeter wave in [5]. However, the propagation of millimeter wave signals is sensitive to the environment, such as object obstructions. Or even worst, the obstruction causes the signal transmission to be interrupted. In this case, the ISAC and/or IPAC system cannot work well. To address this issue, reconfigurable intelligent surface (RIS) is proposed to provide an efficient strategy and solution.

RIS, also known as intelligent reflecting surface (IRS), has been considered as a revolutionary technology for wireless networks, which is composed of massive passive components. RIS adjusts phase shifts of the incident electromagnetic wave to reconfigure the wireless environment and build a virtual line-of-sight (VLoS) link for transmission signals [6], [7]. RIS-aided system enables the improvement of both the communication quality and positioning performance in harsh environments [8]. Therefore, the study of the RIS-based IPAC millimeter wave system has important values and significance.

B. Related Works

Recently, a large number of works have explored ISAC and/or IPAC systems. Liu *et al.* [1] and Zhang *et al.* [9] provided a survey about opportunities and challenges of the integrated system. The ISAC/IPAC enables the positioning and communication signals share the resources frequency and hardware, which significantly solves the spectrum scarcity problem and reduces the cost [10]. To this end, Ayyar *et al.* [11] proposed a communication-centred spectrum coexistence scheme to design a communication-radar system. Kumari *et al.* [4] designed a joint signal waveform for adaptive radar communication to improve the efficiency of the system. Liu *et al.* [12] investigated a spectrum sharing problem of radar transmitters. These works reveal the possibilities and advantages of the integrated design.

With the development of intelligent transport, intelligent travel, and unmanned aerial vehicles (UAVs), more attention is being focused on the IPAC system with the millimeter wave, accompanied by a large number of millimeter wave base stations (BSs) already being deployed. Han

et al. [13] proposed a data-aided positioning system and studied the trade-offs of the integrated millimeter wave system. In [14], the authors proposed a robust beamforming scheme for an IPAC millimeter wave system by considering the impact of the positioning error. Kwon *et al.* [15] jointly designed beamforming and power allocation scheme to satisfy both the communication and positioning performance of an IPAC system. In [5], the authors formulated the IPAC model with the Ziv-Zakai bound (ZZB), and analyzed the trade-offs between communication and positioning.

However, millimeter wave is sensitive to the environments, e.g., obstacles. In other words, the communication and positioning functions are not well realized due to the presence of blockages during the propagation path. RIS, which creates a VLoS link to assist in millimeter wave signal transmission. RIS-enabled systems not only enhance the communication quality [16]–[18], but also improve the positioning accuracy [19]–[21]. Specifically, Wu *et al.* [16], [17] analyzed the active and passive beamforming to evaluate the RIS performance in communication. Huang *et al.* [18] investigated the energy efficiency of the wireless network by utilizing RIS components. For the positioning, Abu-Shaban *et al.* [19] designed a low complexity positioning estimator with the assistance of a RIS. Elzanaty *et al.* [20] derived the expression of the Cramér-Rao bound (CRB) for the RIS-aided positioning system, and evaluated the impact of the RIS phase on the theoretical bound. Keykhosravi *et al.* [21] considered the use of a RIS to estimate locations of the mobile user equipment (UE) by designing RIS phase profiles.

In contrast to the individual analysis of communication and positioning performance described above, several works focused on the design of RIS-aided integrated systems. Yu *et al.* [22] proposed a RIS-enabled integrated framework and designed a integrated transmission protocol. Luo *et al.* [23] explored the signal-to-noises (SNRs) of the radar detection and user communication by deploying a RIS, and demonstrated the advantages offered by the RIS through simulations. Hu *et al.* [24] designed a robust RIS-aided communication system by considering uncertain UE locations, and showed that the quality of service (QoS) requirement can be satisfied with the assistance of the RIS. He *et al.* [25] considered both the positioning accuracy and data rate by designing adaptive RIS phase shifts. Luan *et al.* [26] derived the squared position error bound (PEB) with a RIS, and formulated the integrated system by minimizing the PEB while guaranteeing the achievable data rate constraint in the case of VLoS only. However, research related to joint beamforming design is limited for an IPAC system with RIS.

C. Main Contributions

Inspired by the above discussions, in this paper, we formulate a RIS-enabled IPAC millimeter wave system and jointly optimize the active beamforming and passive beamforming to simultaneously satisfy both the data rate and positioning accuracy requirements. The main contributions of this paper are summarized as follows:

- We propose a RIS-enabled IPAC scheme in a multi-user multi-input single-output (MISO) millimeter wave system. In this system, we derive the explicit expressions of the CRB and PEB for each UE based on the time-of-arrival (ToA) estimation, and use the PEB as the positioning metric for the integrated design.
- We formulate an optimization problem by optimizing the active beamforming in the BS and passive beamforming in the RIS to design the IPAC system. The optimization problem aims to minimize the total transmit power subject to the achievable data rate and PEB constraints. Specifically, in terms of the passive beamforming optimization, we respectively consider the discrete and continuous RIS phase shifts.
- We propose an efficient two-stage algorithm to solve the formulated problem. In the first stage, we aim to optimize the RIS phase shift by using the exhaustive search method for the discrete RIS phase shift case, and using the semidefinite relaxation (SDR) method for the continuous RIS phase shift case. In the second stage, based on the obtained RIS phase, we again use the SDR method to optimize the transmit beamforming in the BS.
- We conduct extensive simulations to demonstrate the performance of the proposed RIS-enabled IPAC system. Specifically, we set different transmission environments, namely, obstruction scenarios, to evaluate the system capability. The results show that the integrated system is effective in both achievable data rate and theoretical positioning error lower bound.

Notations: Boldfaced lowercase and uppercase letters represent vectors and matrices, respectively. $\Re\{\cdot\}$ denotes real part. $[\mathbf{a}]_i$ denotes the i th element in the vector \mathbf{a} and $[\mathbf{A}]_{i,j}$ denotes the (i, j) th element in the matrix \mathbf{A} . The $\text{rank}(\cdot)$, $\text{tr}\{\cdot\}$, $|\cdot|$, $\|\cdot\|$, $(\cdot)^T$, $(\cdot)^H$, and $(\cdot)^{-1}$ denote rank, trace, absolute value, 2-norm, transpose, complex transpose, and inverse operations, respectively. $\mathbf{A} \succeq \mathbf{B}$ means that matrix $\mathbf{A} - \mathbf{B}$ is positive semidefinite. $\mathbb{E}\{\cdot\}$ and $\text{Pr}\{\cdot\}$ denote the expectation and the probability operator, respectively. \mathbf{I} is the identity matrix and $\mathbf{1}_N$ is a $N \times 1$ vector with all elements being ones. The key notations and acronyms are listed in Table. I and Table II, respectively.

TABLE I
SUMMARY OF KEY NOTATIONS

Notations	Description
$\mathbf{w}_{n,k}$	Beamforming vector in the BS
n, k	n th subcarrier and k th UE
Φ	RIS reflection-coefficient matrix
\mathbf{v}	RIS phase shift vector
$\mathbf{h}_{d,n,k}$	Channel from the BS to the UE
$\mathbf{h}_{r,n,k}$	Channel from the RIS to the UE
\mathbf{G}_n	Channel from the BS to the RIS
χ_k	Obstruction indicator
γ_k, \mathcal{P}_k	SINR and PEB
R_k	Achievable data rate
q	Quantization bits number
Δ_f	Subcarrier spacing
r_k	Data rate requirement
δ_k	PEB threshold

TABLE II
SUMMARY OF MAIN ACRONYMS

Acronyms	Description
ISAC	Integrated sensing and communication
IPAC	Integrated positioning and communication
RIS	Reconfigurable intelligent surface
MU-MISO	Multi-user multi-input single-output
CRB	Cramér-Rao bound
PEB	Position error bound
SINR	Signal-to-noise-plus-interference ratio
CSI	Channel state information
FIM	Fisher information matrix
EFIM	Equivalent Fisher information matrix
SDR	Semidefinite relaxation

II. SYSTEM MODEL

In this section, we introduce the system model of the RIS-enabled IPAC system. Based on this system, we formulate the signal transmission model, derive the positioning metric and communication metric.

A. System Setup

As shown in Fig. 1, we consider a RIS-enabled MU-MISO system. The system consists of a multi-antenna BS, a RIS, and K single-antenna UEs. The BS is equipped with N_t antenna elements of a uniform planar array (UPA) and the RIS is equipped with M reflect elements. The locations of the BS, the RIS, and the k th UE are denoted as $\mathbf{p} \in \mathbb{R}^3$, $\mathbf{r} \in \mathbb{R}^3$, and $\mathbf{u}_k \in \mathbb{R}^3$, respectively. For simplicity, we assume that there is no rotation between the BS and RIS.

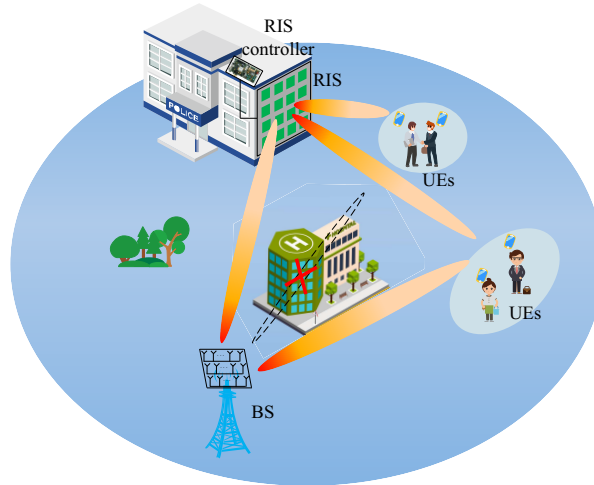


Fig. 1. Illustration of the system.

Moreover, to evaluate the theoretical performance of the IPAC system, without loss of generality, we have follows assumptions: 1) We assume that the channel state information (CSI) of LoS (BS-UE) and VLoS (BS-RIS-UE) links is perfectly known at the BS. 2) We assume that only the direct signals and reflected signals by the RIS are considered, while the other multipath signals reflected by obstacles are negligible. 3) We assume that the channels involved are quasi-static.

B. Signal Transmission Model

Considering an orthogonal frequency division multiplexing (OFDM) transmit system with N subcarrier, each subcarrier consists of positioning and communication information in the

IPAC system, namely, the positioning and communication share the same beams [27], [28]. The transmit signal of the n th subcarrier and the k th UE is denoted as $\mathbf{w}_{n,k}s_{n,k}$, where $\mathbf{w}_{n,k}$ is the active beamforming vector in the BS. Without loss of generality, the data signals $s_{n,k}$ has the following assumptions: 1) $s_{n,k}$ intendeds to different users are uncorrelated, i.e., $\mathbb{E}\{s_{n,i}^*s_{n,j}\} = 0$ for $i \neq j$. 2) $s_{n,k}$ has the unit amplitude, i.e., $\mathbb{E}\{|s_{n,k}|^2\} = 1$.

Considering that the direct LoS paths of several UEs are not available due to obstacles, the received signal $y_{n,k}$ of the n th subcarrier and the k th UE is given as

$$y_{n,k} = \left(\chi_k \mathbf{h}_{d,n,k}^H + \mathbf{h}_{r,n,k}^H \Phi \mathbf{G}_n\right) \sum_{i=1}^K \mathbf{w}_{n,i} s_{n,i} + w_k, \quad (1)$$

where $\chi_k \in \{0, 1\}$ is the obstruction indicator, $\chi_k = 0$ represents the LoS link is obstructed and $\chi_k = 1$ represents the LoS link is available, $\mathbf{h}_{d,n,k} \in \mathbb{C}^{N_t}$, $\mathbf{h}_{r,n,k} \in \mathbb{C}^M$, and $\mathbf{G}_n \in \mathbb{C}^{M \times N_t}$ are respectively denoted as channels from the BS to the k th UE, from the RIS to the k th UE, and from the BS to the RIS of the n th subcarrier, $\Phi \triangleq \text{diag}\{\mathbf{v}\}$ is the reflection-coefficient matrix of the RIS, $\mathbf{v} = \frac{1}{\sqrt{M}}[e^{j\vartheta_1}, \dots, e^{j\vartheta_M}]^T$, $\vartheta_m, \forall m$ is the phase shift, and w_k is the additive white Gaussian noise (AWGN) with zero mean and two-sided power spectral density $N_0/2$. In term of the phase shift of the RIS, we have $|\mathbf{v}_m| = \frac{1}{\sqrt{M}}, \forall m$ for the continuous phase shift, and have $\vartheta_m = \frac{2\pi l}{L}, l \in \mathcal{L} \triangleq \{0, \dots, L-1\}$ for the discrete phase shift, where $L = 2^q$ is the number of phase shift levels and q represents the number of the quantization bits.

For the following discussion, we write the expressions of $\mathbf{h}_{d,n,k}$ and $\mathbf{h}_{r,n,k}$ as

$$\mathbf{h}_{d,n,k}^H = g_{d,n,k} e^{-j2\pi n \Delta_f \tau_{d,k}} \mathbf{a}_{d,n}^H(\phi_{d,k}, \theta_{d,k}), \quad (2a)$$

$$\mathbf{h}_{r,n,k}^H = g_{r,n,k} e^{-j2\pi n \Delta_f \tau_{r,k}} \mathbf{a}_{r,n}^H(\phi_{r,k}, \theta_{r,k}), \quad (2b)$$

where $g_{d,n,k}$ and $g_{r,n,k}$ are complex channel gains of the BS-UE link and the RIS-UE link for the n th subcarrier and the k th UE, respectively, $\tau_{d,k}$ and $\tau_{r,k}$ are corresponding delay, $\mathbf{a}_{d,n}(\phi_{d,k}, \theta_{d,k})$ and $\mathbf{a}_{r,n}(\phi_{r,k}, \theta_{r,k})$ are antenna response vectors in BS and RIS, given by

$$\mathbf{a}_{d,n}(\phi_{d,k}, \theta_{d,k}) = e^{j\Delta_B^T \boldsymbol{\kappa}_n(\phi_{d,k}, \theta_{d,k})}, \quad (3a)$$

$$\mathbf{a}_{r,n}(\phi_{r,k}, \theta_{r,k}) = e^{j\Delta_R^T \boldsymbol{\kappa}_n(\phi_{r,k}, \theta_{r,k})}, \quad (3b)$$

where $\Delta_B \in \mathbb{R}^{3 \times N_t}$ and $\Delta_R \in \mathbb{R}^{3 \times M}$ are denoted as the coordinates of the antenna elements in BS and RIS, respectively, $\phi_{d,k}$ and $\theta_{d,k}$ are azimuth and elevation angles in the AoD of the BS

to the k th UE, $\phi_{r,k}$ and $\theta_{r,k}$ are azimuth and elevation angles in the AoD of the RIS to the k th UE. Considering the spatial-wideband effect, we have

$$\boldsymbol{\kappa}_n(\phi, \theta) = \frac{2\pi}{\lambda_n} [\sin \theta \cos \phi, \sin \theta \sin \phi, \cos \theta]^T, \quad (4)$$

where λ_n is wavelength of the n th subcarrier, expressed as

$$\lambda_n = \frac{c}{f_c + n\Delta_f}, \quad (5)$$

where c is the speed of light, f_c is the carrier frequency, and Δ_f is the subcarrier spacing.

C. Metrics

The proposed IPAC system consists of positioning and communication. In this subsection, we derive metrics to evaluate these two parts, which helps us to jointly design the integrated system.

1) *Positioning Metric*: For the positioning performance, the CRB and PEB are most commonly used to evaluate the theoretical lower bound of an unbiased estimator. Thus, we derive the explicit expressions of the CRB and PEB for each UE. For the notation convenience, we remove the subscript k in deriving the CRB. Moreover, we consider the ToA-based positioning method, thus, we rewrite the received signal in (1) as

$$y_n = \chi \alpha_{d,n} e^{-j2\pi n \Delta_f \tau_d} + \alpha_{r,n} e^{-j2\pi n \Delta_f \tau_r} + w, \quad (6)$$

where

$$\alpha_{d,n} \triangleq \sum_{i=1}^K g_{d,n} \mathbf{a}_{d,n}^H(\phi_d, \theta_d) \mathbf{w}_{n,i} s_{n,i}, \quad (7a)$$

$$\alpha_{r,n} \triangleq \sum_{i=1}^K g_{r,n} \mathbf{a}_{r,n}^H(\phi_r, \theta_r) \Phi \mathbf{G}_n \mathbf{w}_{n,i} s_{n,i}. \quad (7b)$$

Define the channel related unknown parameter $\boldsymbol{\eta}$ as

$$\boldsymbol{\eta} \triangleq [\tau_d, \tau_r, \alpha_{d,n}^R, \alpha_{d,n}^I, \alpha_{r,n}^R, \alpha_{r,n}^I]^T, \quad (8)$$

where the superscripts R and I in (8) are denoted as the real and imaginary parts, respectively.

The mean square error (MSE) of the unbiased estimation $\hat{\boldsymbol{\eta}}$ of $\boldsymbol{\eta}$ is given by

$$\mathbb{E} \left\{ (\hat{\boldsymbol{\eta}} - \boldsymbol{\eta}) (\hat{\boldsymbol{\eta}} - \boldsymbol{\eta})^T \right\} \succeq \mathbf{J}_{\boldsymbol{\eta}}^{-1}, \quad (9)$$

where $\mathbf{J}_\eta \in \mathbb{C}^{6 \times 6}$ is the Fisher information matrix (FIM). Due to the fact that the AWGN is used in the transmission signal model [29], each element in \mathbf{J}_η is calculated by [30]

$$[\mathbf{J}_\eta]_{k_1, k_2} \triangleq \frac{2}{N_0} \sum_{n=1}^N \Re \left\{ \frac{\partial \boldsymbol{\mu}_n^H}{\partial k_1} \frac{\partial \boldsymbol{\mu}_n}{\partial k_2} \right\}, \quad (10)$$

where $k_1, k_2 \in \boldsymbol{\eta}$, and $\boldsymbol{\mu}_n$ is the noiseless part of (6).

Then, we transform the channel related FIM \mathbf{J}_η into the location related FIM $\mathbf{J}_{\tilde{\boldsymbol{\eta}}} \in \mathbb{C}^{7 \times 7}$. Specifically, define the location related unknown parameter $\tilde{\boldsymbol{\eta}}$ as

$$\tilde{\boldsymbol{\eta}} \triangleq [\mathbf{u}, \alpha_{d,n}^R, \alpha_{d,n}^I, \alpha_{r,n}^R, \alpha_{r,n}^I]^T. \quad (11)$$

The location related FIM $\mathbf{J}_{\tilde{\boldsymbol{\eta}}}$ is calculated by $\mathbf{J}_{\tilde{\boldsymbol{\eta}}} = \boldsymbol{\Upsilon} \mathbf{J}_\eta \boldsymbol{\Upsilon}^T$, where $\boldsymbol{\Upsilon} \triangleq \partial \boldsymbol{\eta} / \partial \tilde{\boldsymbol{\eta}}$. Finally, the equivalent FIM (EFIM) \mathbf{J}_p^e can be obtained from $\mathbf{J}_{\tilde{\boldsymbol{\eta}}}$ based on the Schur's complement [31], [32]. The derivation details of the channel related FIM \mathbf{J}_η , the location related FIM $\mathbf{J}_{\tilde{\boldsymbol{\eta}}}$, and the EFIM \mathbf{J}_p^e are shown in Appendix.

Therefore, the explicit expression of the EFIM $\mathbf{J}_{p,k}^e$ of the k th UE is given as

$$\mathbf{J}_{p,k}^e = \chi_k \mathbf{J}_{d,k} + \mathbf{J}_{r,k}, \quad (12)$$

where $\mathbf{J}_{d,k}$ and $\mathbf{J}_{r,k}$ are respectively denoted as the individual EFIMs of the LoS and VLoS paths, which is consistent with [33], [34], given by

$$\mathbf{J}_{d,k} \triangleq \frac{8\pi^2 \Delta_f^2}{c^2} \sum_{n=1}^N n^2 \rho_{d,n,k}(\mathbf{w}_{n,k}) \boldsymbol{\Psi}_{d,k}, \quad (13a)$$

$$\mathbf{J}_{r,k} \triangleq \frac{8\pi^2 \Delta_f^2}{c^2} \sum_{n=1}^N n^2 \rho_{r,n,k}(\mathbf{w}_{n,k}, \boldsymbol{\Phi}) \boldsymbol{\Psi}_{r,k}, \quad (13b)$$

where $\boldsymbol{\Psi}_{d(r),k} = \mathbf{q}_{d(r),k} \mathbf{q}_{d(r),k}^T$, $\mathbf{q}_{d(r),k} \triangleq [\sin \theta_{d(r),k} \cos \phi_{d(r),k}, \sin \theta_{d(r),k} \sin \phi_{d(r),k}, \cos \theta_{d(r),k}]^T$, and

$$\rho_{d,n,k}(\mathbf{w}_{n,k}) \triangleq \frac{\sum_{i=1}^K |\mathbf{h}_{d,n,k}^H \mathbf{w}_{n,i}|^2}{N_0}, \quad (14a)$$

$$\rho_{r,n,k}(\mathbf{w}_{n,k}, \boldsymbol{\Phi}) \triangleq \frac{\sum_{i=1}^K |\mathbf{h}_{r,n,k}^H \boldsymbol{\Phi} \mathbf{G}_n \mathbf{w}_{n,i}|^2}{N_0}. \quad (14b)$$

To this end, we write the explicit expression of the CRB for the k th UE as

$$\text{CRB}_k = \text{tr} \{ (\chi_k \mathbf{J}_{\text{d},k} + \mathbf{J}_{\text{r},k})^{-1} \}, \forall k. \quad (15)$$

Then, the PEB $\mathcal{P}_k(\mathbf{w}_{n,k}, \Phi)$ of the k th UE is given by

$$\mathcal{P}_k(\mathbf{w}_{n,k}, \Phi) = \sqrt{\text{CRB}_k} = \sqrt{\text{tr} \{ (\chi_k \mathbf{J}_{\text{d},k} + \mathbf{J}_{\text{r},k})^{-1} \}}, \forall k. \quad (16)$$

2) *Communication Metric*: For the communication service, we derive the achievable data rate for each UE as the metric. Based on the received signal in (1), the signal-to-noise-plus-noise (SINR) γ_k of the k th UE is given by

$$\gamma_k = \frac{\sum_{n=1}^N |(\chi_k \mathbf{h}_{\text{d},n,k}^H + \mathbf{h}_{\text{r},n,k}^H \Phi \mathbf{G}_n) \mathbf{w}_{n,k}|^2}{\sum_{j=1, j \neq k}^K \sum_{n=1}^N |(\chi_k \mathbf{h}_{\text{d},n,k}^H + \mathbf{h}_{\text{r},n,k}^H \Phi \mathbf{G}_n) \mathbf{w}_{n,j}|^2 + N_0}, \forall k. \quad (17)$$

Then, the data rate $R_k(\mathbf{w}_{n,k}, \Phi)$ in bps/Hz of the k th UE is expressed as

$$R_k(\mathbf{w}_{n,k}, \Phi) = \log_2(1 + \gamma_k), \forall k. \quad (18)$$

D. Goal

Our goal is to build an IPAC millimeter wave system by jointly designing active beamforming in the BS and passive beamforming in the RIS. To be more specific, we formulate and solve an optimization problem that aims at minimizing the total transmit power while simultaneously guaranteeing the data rate and positioning accuracy constraints.

III. PROBLEM FORMULATION

The optimization problem for the IPAC system design is formulated as

$$\min_{\mathbf{w}_{n,k}, \Phi} \sum_{k=1}^K \sum_{n=1}^N \|\mathbf{w}_{n,k}\|^2 \quad (19a)$$

$$\text{s.t. } R_k(\mathbf{w}_{n,k}, \Phi) \geq r_k, \forall k, \quad (19b)$$

$$\mathcal{P}_k(\mathbf{w}_{n,k}, \Phi) \leq \delta_k, \forall k, \quad (19c)$$

$$\vartheta_m = \frac{2\pi l}{L}, l \in \mathcal{L}, \forall m \quad (\text{or}) \quad |\Phi_{m,m}| = \frac{1}{\sqrt{M}}, \forall m, \quad (19d)$$

where r_k and δ_k are the rate requirement and the PEB threshold of the k th UE, respectively. The constraints (19b) and (19c) guarantee the data rate and the positioning accuracy of each UE respectively, and (19d) is the phase shift constraint for each reflected element in the RIS.

It is easy to find that the optimization problem (19) is hard to be solved because variables $\mathbf{w}_{n,k}$ and Φ are coupled to each other. Thus, we propose an efficient low-complexity two-stage algorithm to decouple the problem into two subproblems. Specifically, we optimize the RIS phase shift in the first stage, and then design the active beamforming vector in the second stage with the given phase shift.

A. Stage I: Optimize Φ

In order to optimize the RIS phase shift Φ , we aim to align with the phase of channels of various UEs. In other words, we focus on solving a weighted sum of the channel gain maximization problem [16]. For the constraints (19b), the goal is to maximize

$$\sum_{k=1}^K \sum_{n=1}^N \frac{\|\chi_k \mathbf{h}_{d,n,k}^H + \mathbf{h}_{r,n,k}^H \Phi \mathbf{G}_n\|^2}{\beta_k N_0} \geq \sum_{k=1}^K \sum_{n=1}^N \frac{\|\chi_k \mathbf{h}_{d,n,k}^H\|^2}{\beta_k N_0} + \frac{\|\mathbf{h}_{r,n,k}^H \Phi \mathbf{G}_n\|^2}{\beta_k N_0}, \quad (20)$$

where $\beta_k \triangleq 2^{r_k} - 1$. For the constraint (19c), the goal is to maximize

$$\sum_{k=1}^K \sum_{n=1}^N \frac{\|\mathbf{h}_{r,n,k}^H \Phi \mathbf{G}_n\|^2}{\beta_k N_0}. \quad (21)$$

Thus, let $\mathbf{h}_{r,n,k}^H \Phi \mathbf{G}_n \triangleq \mathbf{v}^T \text{diag}\{\mathbf{h}_{r,n,k}^H\} \mathbf{G}_n$, the channel gain maximization problem of (20) and (21) can be jointly formulated as

$$\max_{\mathbf{v}} \sum_{k=1}^K \sum_{n=1}^N \frac{\|\mathbf{v}^T \text{diag}\{\mathbf{h}_{r,n,k}^H\} \mathbf{G}_n\|^2}{\beta_k} \quad (22a)$$

$$\text{s.t. } \vartheta_m = \frac{2\pi l}{L}, l \in \mathcal{L}, \forall m \quad (\text{or}) \quad |\mathbf{v}_m| = \frac{1}{\sqrt{M}}, \forall m. \quad (22b)$$

1) *Discrete Phase Shift Case:* For the discrete phase shift case, basically, we can directly solve the subproblem (22) based on the exhaustive search method. Let $\mathbf{C}_{n,k} \triangleq \text{diag}\{\mathbf{h}_{r,n,k}^H\} \mathbf{G}_n$, the optimization problem of (22) with discrete phase shift is converted into

$$\max_{\mathbf{v}} \sum_{k=1}^K \sum_{n=1}^N \frac{\|\mathbf{v}^T \mathbf{C}_{n,k}\|^2}{\beta_k} \quad (23a)$$

$$\text{s.t. } \vartheta_m = \frac{2\pi l}{L}, l \in \mathcal{L}, \forall m. \quad (23b)$$

Then, for a given $m \in \{1, \dots, M\}$, by fixing ϑ_i 's, $\forall i \neq m$, the objective function of (23) is linear with respect to $e^{j\vartheta_m}$, which can be written as [17], [35]

$$2\Re \{e^{j\vartheta_m} \zeta_m\} + \sum_{k=1}^K \sum_{n=1}^N \frac{1}{\beta_k} \left(\sum_{i=1, i \neq m}^M \sum_{\iota=1, \iota \neq m}^M [\mathbf{A}_{n,k}]_{i,\iota} e^{j(\vartheta_i - \vartheta_\iota)} + [\mathbf{A}_{n,k}]_{m,m} \right), \quad (24)$$

where $\mathbf{A}_{n,k} \triangleq \mathbf{C}_{n,k} \mathbf{C}_{n,k}^H$ and $\zeta_m = \sum_{k=1}^K \sum_{n=1}^N \sum_{i=1, i \neq m}^M \frac{1}{\beta_k} [\mathbf{A}_{n,k}]_{m,i} e^{-j\vartheta_i} = |\zeta_m| e^{-j\xi_m}$. Thus, the optimal m th phase shift $\hat{\vartheta}_m$ is given by

$$\hat{\vartheta}_m = \arg \min_{\vartheta} |\vartheta - \xi_m|. \quad (25)$$

2) *Continuous Phase Shift Case:* For the continuous phase shift case, the subproblem (22) is non-convex, so as to be solved by using the SDR method. Specifically, we define the covariance matrix $\mathbf{V} \triangleq \mathbf{v}\mathbf{v}^H$, and reformulate the optimization subproblem (22) as

$$\max_{\mathbf{V}} \sum_{k=1}^K \sum_{n=1}^N \frac{\text{tr}\{\mathbf{V} \mathbf{A}_{n,k}\}}{\beta_k} \quad (26a)$$

$$\text{s.t. } \mathbf{V}_{m,m} = \frac{1}{M}, \forall m, \quad (26b)$$

$$\mathbf{V} \succeq \mathbf{0}, \quad (26c)$$

$$\text{rank}(\mathbf{V}) = 1. \quad (26d)$$

By dropping the rank-1 constraint (26d), the problem (26) is equivalent to

$$\max_{\mathbf{V}} \sum_{k=1}^K \sum_{n=1}^N \frac{\text{tr}\{\mathbf{V} \mathbf{A}_{n,k}\}}{\beta_k} \quad (27a)$$

$$\text{s.t. } (26b), (26c).$$

The optimal solutions \mathbf{V}^* can be obtained by using convex optimization solvers such as CVX [36]. Due to the fact that the SDR may not be tight, we can extract the feasible solution $\hat{\mathbf{v}}$ from \mathbf{V}^* based on the Gaussian randomization method [37].

B. Stage II: Optimize $\mathbf{w}_{n,k}$ with the Given Φ

For the given Φ , the problem (19) is converted into

$$\min_{\mathbf{w}_{n,k}} \sum_{k=1}^K \sum_{n=1}^N \|\mathbf{w}_{n,k}\|^2 \quad (28a)$$

$$\text{s.t.} \quad \log_2 \left(1 + \frac{\sum_{n=1}^N |\mathbf{g}_{n,k}^H \mathbf{w}_{n,k}|^2}{\sum_{j=1, j \neq k}^K \sum_{n=1}^N |\mathbf{g}_{n,k}^H \mathbf{w}_{n,j}|^2 + N_0} \right) \geq r_k, \forall k, \quad (28b)$$

$$\text{tr} \left\{ \left(\frac{8\pi^2 \Delta_f^2}{c^2} \sum_{n=1}^N n^2 \chi_k \rho_{d,n,k} (\mathbf{w}_{n,k}) \Psi_{d,k} + n^2 \rho_{r,n,k} (\mathbf{w}_{n,k}) \Psi_{r,k} \right)^{-1} \right\} \leq \delta_k^2, \forall k, \quad (28c)$$

where $\mathbf{g}_{n,k}^H \triangleq \chi_k \mathbf{h}_{d,n,k}^H + \mathbf{h}_{r,n,k}^H \Phi \mathbf{G}_n$.

Similarly, by defining the covariance matrix $\mathbf{W}_{n,k} \triangleq \mathbf{w}_{n,k} \mathbf{w}_{n,k}^H$ and using the SDR method, the subproblem (28) is rewritten after dropping the rank-1 constraint as

$$\min_{\mathbf{W}_{n,k}} \sum_{k=1}^K \sum_{n=1}^N \text{tr} \{ \mathbf{W}_{n,k} \} \quad (29a)$$

$$\text{s.t.} \quad \log_2 \left(1 + \frac{\sum_{n=1}^N \mathbf{g}_{n,k}^H \mathbf{W}_{n,k} \mathbf{g}_{n,k}}{\sum_{j=1, j \neq k}^K \sum_{n=1}^N \mathbf{g}_{n,k}^H \mathbf{W}_{n,j} \mathbf{g}_{n,k} + N_0} \right) \geq r_k, \forall k, \quad (29b)$$

$$\text{tr} \left\{ \left(\frac{8\pi^2 \Delta_f^2}{c^2} \sum_{n=1}^N n^2 \chi_k \rho_{d,n,k} (\mathbf{W}_{n,k}) \Psi_{d,k} + n^2 \rho_{r,n,k} (\mathbf{W}_{n,k}) \Psi_{r,k} \right)^{-1} \right\} \leq \delta_k^2, \forall k, \quad (29c)$$

$$\mathbf{W}_{n,k} \succeq \mathbf{0}, \forall n, k. \quad (29d)$$

For the constraint (29b), by applying the convex semidefinite program (SDP) method [38], it can be rewritten as

$$\sum_{n=1}^N \text{tr} \{ \mathbf{g}_{n,k}^H \mathbf{W}_{n,k} \mathbf{g}_{n,k} \} \geq \sum_{j=1, j \neq k}^K \sum_{n=1}^N \beta_k \text{tr} \{ \mathbf{g}_{n,k}^H \mathbf{W}_{n,j} \mathbf{g}_{n,k} \} + \beta_k N_0, \forall k. \quad (30)$$

Furthermore, for the constraint (29c), we introduce variable matrices $\Lambda_k, \forall k$, and apply the Schur's complement to transform it into a series of linear matrix inequalities (LMIs) [39], which

can be rewritten as

$$\begin{bmatrix} \mathbf{\Lambda}_k & & & \mathbf{I} \\ & \mathbf{I} & & \\ & & \frac{8\pi^2\Delta_f^2}{c^2} \sum_{n=1}^N n^2 \chi_k \rho_{d,n,k}(\mathbf{W}_{n,k}) \mathbf{\Psi}_{d,k} + n^2 \rho_{r,n,k}(\mathbf{W}_{n,k}) \mathbf{\Psi}_{r,k} & \\ & & & \end{bmatrix} \succeq \mathbf{0}, \forall k, \quad (31a)$$

$$\text{tr}\{\mathbf{\Lambda}_k\} \leq \delta_k^2, \forall k, \quad (31b)$$

$$\mathbf{\Lambda}_k \succeq \mathbf{0}, \forall k. \quad (31c)$$

Therefore, the solutions of the subproblem (28) can be obtained by solving

$$\min_{\mathbf{W}_{n,k}, \mathbf{\Lambda}_k} \sum_{k=1}^K \sum_{n=1}^N \text{tr}\{\mathbf{W}_{n,k}\} \quad (32a)$$

$$\text{s.t.} \quad (29d), (30), (31a), (31b), (31c).$$

The optimal solutions $\mathbf{W}_{n,k}^*$ of the optimization problem (32) can be obtained by using CVX tools. Then, we extract feasible solutions $\hat{\mathbf{w}}_{n,k}$ from $\mathbf{W}_{n,k}^*$ based on the Gaussian randomization method.

The whole two-stage algorithm for jointly optimizing the active beamforming vector $\mathbf{w}_{n,k}$ and the passive RIS phase shift \mathbf{v} is shown in Algorithm 1.

Algorithm 1: Proposed two-stage algorithm to solve the problem (19)

Input: $r_k > 0, \delta_k > 0, \forall k$

Output: Beamforming vector $\hat{\mathbf{w}}_{n,k}$ and RIS phase shift $\hat{\mathbf{v}}$

// (Stage I):

- 1 (Discrete phase shift case): Obtain the solution $\hat{\mathbf{v}}$ by solving the subproblem (25) with the exhaustive search method;
 - 2 (Continuous phase shift case): Obtain the solution \mathbf{V}^* by solving the subproblem (27) with the SDR method;
 - 3 Exact feasible solutions $\hat{\mathbf{v}}$ from \mathbf{V}^* based on the Gaussian randomization method;
- // (Stage II):
- 4 Obtain the solution $\mathbf{W}_{n,k}^*$ by solving the subproblem (32) with the SDR method;
 - 5 Exact feasible solutions $\hat{\mathbf{w}}_{n,k}$ from $\mathbf{W}_{n,k}^*$ based on the Gaussian randomization method;
 - 6 **return** $\hat{\mathbf{w}}_{n,k}$ and $\hat{\mathbf{v}}$;
-

C. Complexity Analysis

In summary, we can solve the optimization problem (19) by dividing it into two subproblems in Stage I and Stage II. The complexity of solving the subproblem in Stage I with the discrete

RIS phase shift and with the continuous RIS phase shift is $\mathcal{O}(ML)$ and $\mathcal{O}(M^{4.5} \log(1/\epsilon_1))$, respectively, where $\epsilon_1 > 0$ is the predefined solution accuracy of the problem (27). The complexity of solving the subproblem in Stage II is $\mathcal{O}((NKN_t)^{4.5} \log(1/\epsilon_2))$, where $\epsilon_2 > 0$ is the predefined solution accuracy of the problem (32) [37]. Compared to the conventional alternating optimization (AO) method [16], [17], [35], the adopted two-stage algorithm has a low complexity because the latter is only alternatively optimized once.

IV. SIMULATION RESULTS

A. Simulation Setup

In this section, we conduct simulations to evaluate the performance of the proposed IPAC system. Generally, in following simulations, we set the data rate requirement r_k and the PEB threshold δ_k to be the same for every UE, the values of which are given specifically in each simulation below. The other key parameters are listed in Table III.

TABLE III
PARAMETER CONFIGURATIONS OF SIMULATIONS

Frequency f_c	30 GHz
BS antenna number N_t	4×4
UE number K	3
RIS size M	12×12
Subcarrier spacing Δ_f	120 kHz
Subcarrier number N	1000
Bandwidth $N\Delta_f$	120 MHz
PSD of noise N_0	-174 dBm/Hz
Noise figure	8 dB

Moreover, we respectively conduct simulations in following scenarios:

- 1) Scenario 1: All direct links to UEs are available, namely, we set $\chi = [1, 1, 1]^T$.
- 2) Scenario 2: The second UE's direct link is obstructed, namely, we set $\chi = [1, 0, 1]^T$.
- 3) Scenario 3: All direct links to UEs are obstructed, namely, we set $\chi = [0, 0, 0]^T$.

B. Evaluation for Scenario 1

In Scenario 1, all direct links to UEs are not obstructed. The signal propagation illustration and the coordinates of the BS, UEs, and RIS are shown in Fig. 2.

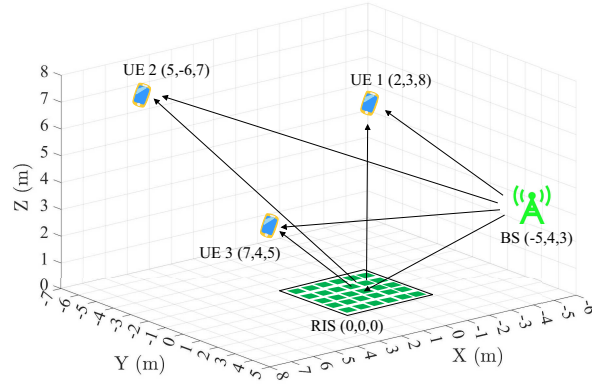


Fig. 2. Illustration of the signal propagation in Scenario 1.

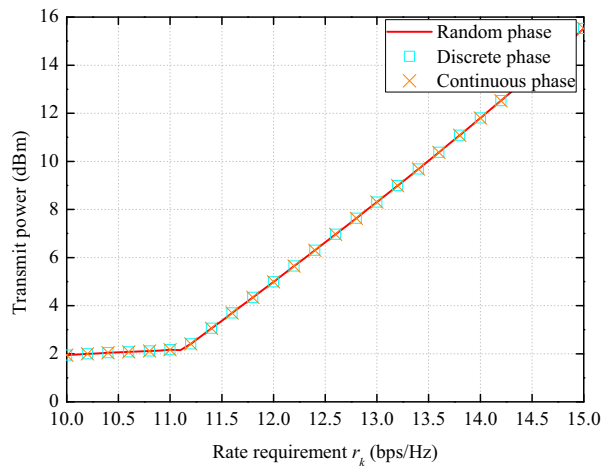


Fig. 3. Scenario 1: Transmit power versus the rate requirement r_k with various RIS phase shift designs.

Fig. 3 demonstrates the total transmit power versus the data rate requirement r_k with various RIS phase shift designs, where $\delta_k = 0.01$ m. We can observe that the transmit power first remains stable and then increases with r_k . The reason is that the transmit power is first limited by the positioning constraint, i.e., PEB threshold δ_k . As the rate requirement r_k increases, the transmit power turns to be limited by the communication constraint. Moreover, it is shown that the curves for the random RIS phase shift¹, the discrete RIS phase shift with the quantization bits number $q = 2$, and the continuous RIS phase shift overlap. This can be explained by the fact that beams in the BS are directed towards the corresponding UEs and the signals reflected by the RIS are negligible, since the path loss in the LoS path is much smaller compared to the VLoS path.

¹The random RIS phase shift indicates that the phase shift in Φ of the RIS is randomly distributed over $[0, 2\pi)$, i.e., $\vartheta_m \sim \mathcal{U}(0, 2\pi)$, $\forall m$.

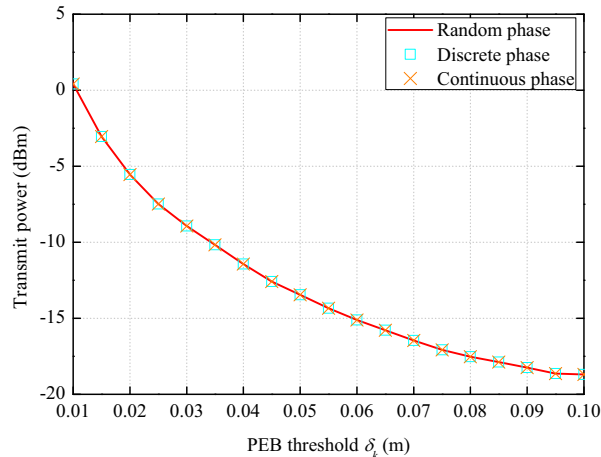


Fig. 4. Scenario 1: Transmit power versus the PEB threshold δ_k with various RIS phase shift designs.

Fig. 4 depicts the total transmit power versus the PEB threshold δ_k with various RIS phase shift designs, where $r_k = 5$ bps/Hz. We can observe that the transmit power decreases as the PEB threshold δ_k increases. This can easily be explained by the fact that the performance of the IPAC system is at this point limited by the positioning constraint. More power is required in order to achieve higher positioning accuracy. In addition, the curves for the various RIS phase shifts overlap with the same reason as in Fig. 3.

C. Evaluation for Scenario 2

In Scenario 2, the direct link of the second UE is obstructed, which is shown in Fig. 5.

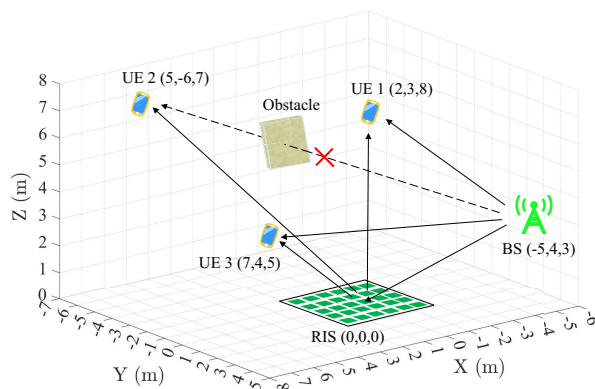


Fig. 5. Illustration of the signal propagation in Scenario 2.

Fig. 6 shows the transmit power versus the data rate requirement r_k with $\delta_k = 0.1$ m. It can obviously be seen that the transmit power significantly increases compared to Fig. 3, even when

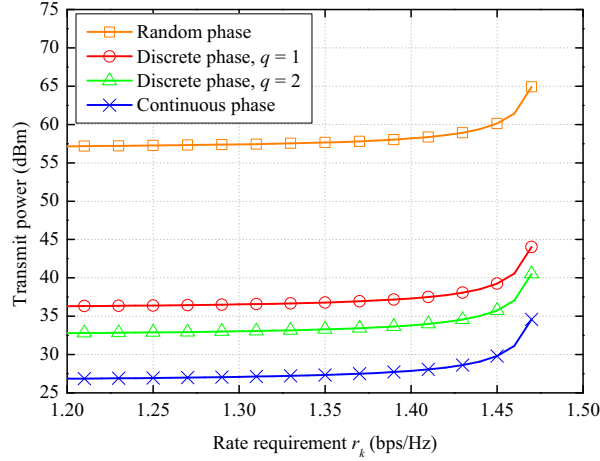


Fig. 6. Scenario 2: Transmit power versus the rate requirement r_k with various RIS phase shift designs.

setting lower data rate requirement r_k and higher PEB threshold δ_k . This is because the path loss of the VLoS path of the second UE is much higher than that of the LoS path, which results in a higher power consumption. Nevertheless, the RIS-aided design makes sense as it enables successful communication and positioning functions for the UE which signal propagation paths are obscured. In addition, overall speaking, the transmit power increases with the rate requirement r_k . More specifically, the power consumption is lower with larger quantization bits number q , while the search complexity in (25) is higher. The lowest power is required for the continuous RIS phase shift design to implement the IPAC system. The results verify the effectiveness of the proposed two-stage algorithm.

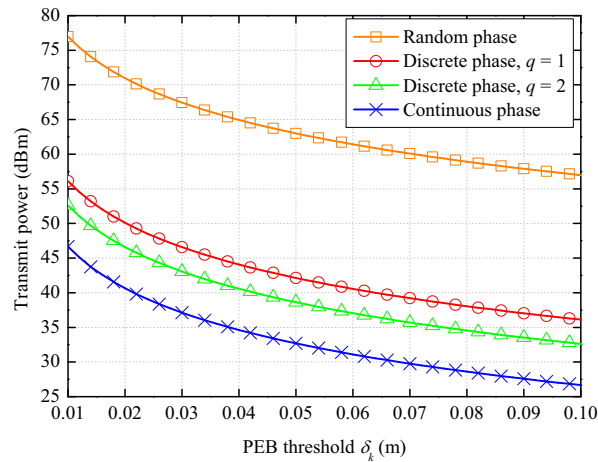


Fig. 7. Scenario 2: Transmit power versus the PEB threshold δ_k with various RIS phase shift designs.

Fig. 7 demonstrates the transmit power versus the PEB threshold δ_k with $r_k = 1$ bps/Hz. We can observe that the drop in the transmit power is obvious as the PEB threshold δ_k increases. It can be explained that in this case the main constraint on the design of the IPAC system is the positioning accuracy requirement. Moreover, not surprisingly, when the design of the RIS phase shift is continuous, the transmit power consumption is minimal, which is consistent with Fig. 6.

D. Evaluation for Scenario 3

In Scenario 3, all direct links to UEs are obstructed, which is shown in Fig. 8. In this case, the interferences between the UEs are significant high because all signals come from the reflected link by the RIS, which only produces a beam in one direction. To compensate for this issue, follow the methods in [40], [41], we divide the RIS into three sub-UPAs to generate three beams, each equipped with $M/3$ reflected elements, as shown in Fig. 9.

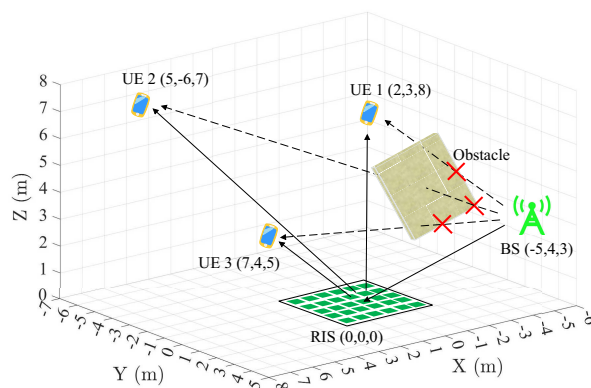


Fig. 8. Illustration of the signal propagation in Scenario 3.

Similarly, we also conduct simulations to evaluate the impact of the data rate requirement r_k and the PEB threshold δ_k on the transmit power in Fig. 10 with $\delta_k = 1$ m and in Fig. 11 with $r_k = 0.1$ bps/Hz, respectively. The transmit power increases with the data rate requirement r_k and decreases with the PEB threshold δ_k . Thus, we can conclude that the proposed RIS-enabled IPAC design is suitable for all cases where transmission paths are blocked.

V. CONCLUSIONS

In this work, we have formulated an IPAC millimeter wave system with the assistance of a RIS. The active beamforming in the BS and the passive beamforming in the RIS are jointly designed to minimize the total transmit power. Then, we propose to use a series of algorithms to solve

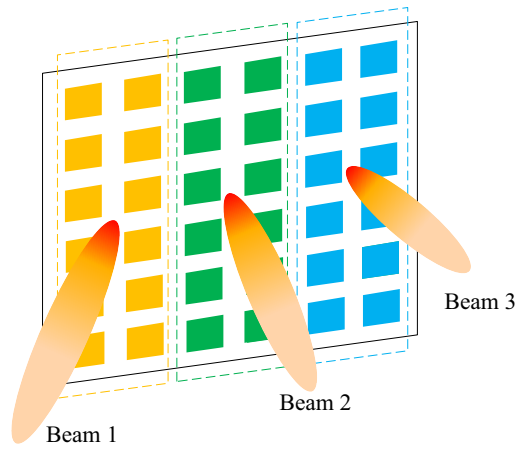


Fig. 9. Illustration of three beams of different directions in a RIS.

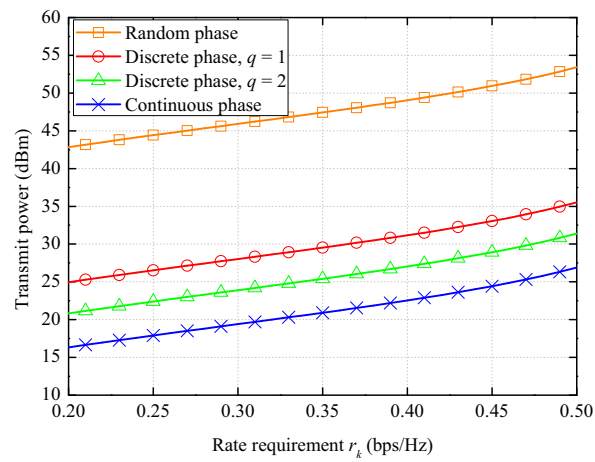


Fig. 10. Scenario 3: Transmit power versus the rate requirement r_k with various RIS phase shift designs.

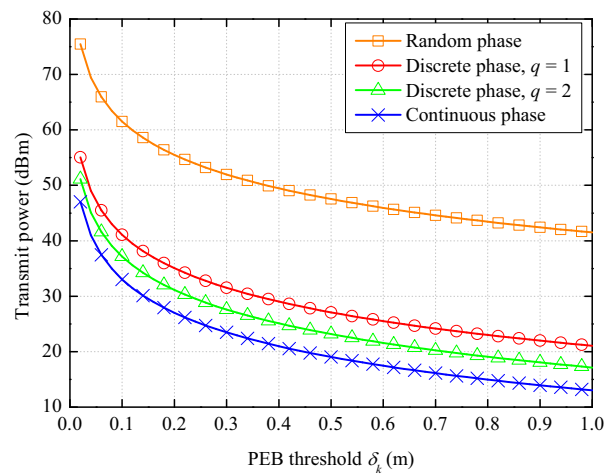


Fig. 11. Scenario 3: Transmit power versus the PEB threshold δ_k with various RIS phase shift designs.

the formulated optimization problem. Finally, numerical results demonstrate the effectiveness of the integrated system by varying the system parameters.

APPENDIX

In this appendix, we derive the explicit expressions of the FIM and EFIM. According to (10), the FIM $\mathbf{J}_\eta \in \mathbb{C}^{6 \times 6}$ can be structured as

$$\mathbf{J}_\eta \triangleq \begin{bmatrix} J_{\tau_d \tau_d} & \cdots & J_{\tau_d \alpha_{r,n}^I} \\ \vdots & \ddots & \vdots \\ J_{\alpha_{r,n}^I \tau_d} & \cdots & J_{\alpha_{r,n}^I \alpha_{r,n}^I} \end{bmatrix}, \quad (33)$$

Specifically, the first-order partial derivatives in (10) are given as

$$\frac{\partial \mu_n}{\partial \tau_d} = -j2\pi n \Delta_f \chi \alpha_{d,n} e^{-j2\pi n \Delta_f \tau_d}, \quad (34a)$$

$$\frac{\partial \mu_n}{\partial \tau_r} = -j2\pi n \Delta_f \chi \alpha_{r,n} e^{-j2\pi n \Delta_f \tau_r}, \quad (34b)$$

$$\frac{\partial \mu_n}{\partial \alpha_{d,n}^R} = \chi e^{-j2\pi n \Delta_f \tau_d}, \quad (34c)$$

$$\frac{\partial \mu_n}{\partial \alpha_{d,n}^I} = j\chi e^{-j2\pi n \Delta_f \tau_d}, \quad (34d)$$

$$\frac{\partial \mu_n}{\partial \alpha_{r,n}^R} = e^{-j2\pi n \Delta_f \tau_r}, \quad (34e)$$

$$\frac{\partial \mu_n}{\partial \alpha_{r,n}^I} = j e^{-j2\pi n \Delta_f \tau_r}. \quad (34f)$$

Based on the above partial derivatives, we can calculate the elements in \mathbf{J}_η as follows

$$J_{\tau_d \tau_d} = \frac{2}{N_0} \sum_{n=1}^N (2\pi n \Delta_f)^2 \chi^2 |\alpha_{d,n}|^2, \quad (35a)$$

$$J_{\tau_d \tau_r} = \frac{2}{N_0} \sum_{n=1}^N \Re \left\{ (2\pi n \Delta_f)^2 \chi \alpha_{d,n}^* \alpha_{r,n} e^{j2\pi n \Delta_f (\tau_d - \tau_r)} \right\}, \quad (35b)$$

$$J_{\tau_d \alpha_{r,n}^R} = \frac{2}{N_0} \sum_{n=1}^N \Re \left\{ j2\pi n \Delta_f \chi \alpha_{d,n}^* e^{j2\pi n \Delta_f (\tau_d - \tau_r)} \right\}, \quad (35c)$$

$$J_{\tau_d \alpha_{r,n}^I} = \frac{2}{N_0} \sum_{n=1}^N \Re \left\{ -2\pi n \Delta_f \chi \alpha_{d,n}^* e^{j2\pi n \Delta_f (\tau_d - \tau_r)} \right\}, \quad (35d)$$

$$J_{\tau_r \tau_r} = \frac{2}{N_0} \sum_{n=1}^N (2\pi n \Delta_f)^2 |\alpha_{r,n}|^2, \quad (35e)$$

$$J_{\tau_r \alpha_{d,n}^R} = \frac{2}{N_0} \sum_{n=1}^N \Re \left\{ j2\pi n \Delta_f \chi \alpha_{r,n}^* e^{j2\pi n \Delta_f (\tau_r - \tau_d)} \right\}, \quad (35f)$$

$$J_{\tau_r \alpha_{d,n}^I} = \frac{2}{N_0} \sum_{n=1}^N \Re \left\{ -2\pi n \Delta_f \chi \alpha_{r,n}^* e^{j2\pi n \Delta_f (\tau_r - \tau_d)} \right\}, \quad (35g)$$

$$J_{\alpha_{d,n}^R \alpha_{r,n}^R} = J_{\alpha_{d,n}^I \alpha_{r,n}^I} = \frac{2}{N_0} \sum_{n=1}^N \chi \Re \left\{ e^{j2\pi n \Delta_f (\tau_d - \tau_r)} \right\}, \quad (35h)$$

$$J_{\alpha_{d,n}^R \alpha_{r,n}^I} = \frac{2}{N_0} \sum_{n=1}^N \chi \Re \left\{ j e^{j2\pi n \Delta_f (\tau_d - \tau_r)} \right\}, \quad (35i)$$

$$J_{\alpha_{d,n}^I \alpha_{r,n}^R} = \frac{2}{N_0} \sum_{n=1}^N \chi \Re \left\{ -j e^{j2\pi n \Delta_f (\tau_d - \tau_r)} \right\}, \quad (35j)$$

$$J_{\alpha_{d,n}^R \alpha_{d,n}^R} = J_{\alpha_{d,n}^I \alpha_{d,n}^I} = \chi^2, \quad (35k)$$

$$J_{\alpha_{r,n}^R \alpha_{r,n}^R} = J_{\alpha_{r,n}^I \alpha_{r,n}^I} = 1. \quad (35l)$$

The rest elements in \mathbf{J}_η are zeros. In addition, according to the analysis results from [33], [34], [42], if a large bandwidth is adopted, which is customary in millimeter wave systems, the components of direct and reflected paths can be considered orthogonal. In this case, we can approximate the FIM \mathbf{J}_η as

$$\mathbf{J}_\eta \approx \text{diag} \left\{ J_{\tau_d \tau_d}, J_{\tau_r \tau_r}, \chi^2, \chi^2, \mathbf{1}_2^T \right\}. \quad (36)$$

Then, we transform the channel related FIM \mathbf{J}_η into the location related FIM $\mathbf{J}_{\tilde{\eta}} \in \mathbb{C}^{7 \times 7}$. The

denoted transform matrix $\Upsilon \in \mathbb{C}^{7 \times 6}$ is given as

$$\Upsilon \triangleq \frac{\partial \boldsymbol{\eta}}{\partial \tilde{\boldsymbol{\eta}}} = \left[\begin{array}{c|c} \left[\begin{array}{cc} \frac{\partial \tau_d}{\partial \mathbf{u}} & \frac{\partial \tau_r}{\partial \mathbf{u}} \end{array} \right] & \mathbf{0}_{3 \times 4} \\ \hline \mathbf{0}_{4 \times 2} & \mathbf{I}_{4 \times 4} \end{array} \right], \quad (37)$$

where

$$\frac{\partial \tau_d}{\partial \mathbf{u}} = \frac{\mathbf{u} - \mathbf{p}}{c \|\mathbf{u} - \mathbf{p}\|}, \quad (38a)$$

$$\frac{\partial \tau_r}{\partial \mathbf{u}} = \frac{\mathbf{u} - \mathbf{r}}{c \|\mathbf{u} - \mathbf{r}\|}. \quad (38b)$$

Thus, the location related FIM $\mathbf{J}_{\tilde{\boldsymbol{\eta}}}$ is given as

$$\mathbf{J}_{\tilde{\boldsymbol{\eta}}} = \Upsilon \mathbf{J}_{\boldsymbol{\eta}} \Upsilon^T \triangleq \left[\begin{array}{c|c} J_{\tau_d \tau_d} \frac{\partial \tau_d}{\partial \mathbf{u}} \frac{\partial \tau_d}{\partial \mathbf{u}^T} + J_{\tau_r \tau_r} \frac{\partial \tau_r}{\partial \mathbf{u}} \frac{\partial \tau_r}{\partial \mathbf{u}^T} & \mathbf{0}_{3 \times 4} \\ \hline \mathbf{0}_{3 \times 4}^T & \mathbf{I}_{4 \times 4} \end{array} \right]. \quad (39)$$

According to Schur's complement, the EFIM \mathbf{J}_p^e of the UE location is given by

$$\mathbf{J}_p^e = J_{\tau_d \tau_d} \frac{\partial \tau_d}{\partial \mathbf{u}} \frac{\partial \tau_d}{\partial \mathbf{u}^T} + J_{\tau_r \tau_r} \frac{\partial \tau_r}{\partial \mathbf{u}} \frac{\partial \tau_r}{\partial \mathbf{u}^T}. \quad (40)$$

REFERENCES

- [1] F. Liu, Y. Cui, C. Masouros, J. Xu, T. X. Han, Y. C. Eldar, and S. Buzzi, "Integrated sensing and communications: Toward dual-functional wireless networks for 6g and beyond," *IEEE J. Sel. Areas Commun.*, vol. 40, no. 6, pp. 1728–1767, Jun. 2022.
- [2] Z. Wei, F. Liu, C. Masouros, N. Su, and A. P. Petropulu, "Toward multi-functional 6G wireless networks: Integrating sensing, communication, and security," *IEEE Commun. Mag.*, vol. 60, no. 4, pp. 65–71, Apr. 2022.
- [3] Z. Feng, Z. Fang, Z. Wei, X. Chen, Z. Quan, and D. Ji, "Joint radar and communication: A survey," *China Communications*, vol. 17, no. 1, pp. 1–27, Jan. 2020.
- [4] P. Kumari, N. J. Myers, and R. W. Heath, "Adaptive and fast combined waveform-beamforming design for mmWave automotive joint communication-radar," *IEEE J. Sel. Top. Signal Process.*, vol. 15, no. 4, pp. 996–1012, Jun. 2021.
- [5] J. Sun, S. Ma, G. Xu, and S. Li, "Trade-off between positioning and communication for millimeter wave systems with Ziv-Zakai bound," *IEEE Trans. Commun.*, Early Access, 2023, doi: 10.1109/TCOMM.2023.3265113.
- [6] P. Liu, Y. Li, W. Cheng, X. Gao, and X. Huang, "Intelligent reflecting surface aided NOMA for millimeter-wave massive MIMO with lens antenna array," *IEEE Trans. Veh. Technol.*, vol. 70, no. 5, pp. 4419–4434, May 2021.
- [7] Y. Liu, Q. Shi, Q. Wu, J. Zhao, and M. Li, "Joint node activation, beamforming and phase-shifting control in IoT sensor network assisted by reconfigurable intelligent surface," *IEEE Trans. Wireless Commun.*, vol. 21, no. 11, pp. 9325–9340, Nov. 2022.
- [8] Z. Li, W. Chen, Q. Wu, H. Cao, K. Wang, and J. Li, "Robust beamforming design and time allocation for IRS-assisted wireless powered communication networks," *IEEE Trans. Commun.*, vol. 70, no. 4, pp. 2838–2852, Apr. 2022.
- [9] J. A. Zhang, M. L. Rahman, K. Wu, X. Huang, Y. J. Guo, S. Chen, and J. Yuan, "Enabling joint communication and radar sensing in mobile networks—a survey," *IEEE Commun. Surveys Tuts.*, vol. 24, no. 1, pp. 306–345, 1st Quart. 2022.

- [10] A. Liu, Z. Huang, M. Li, Y. Wan, W. Li, T. X. Han, C. Liu, R. Du, D. K. P. Tan, J. Lu, Y. Shen, F. Colone, and K. Chetty, "A survey on fundamental limits of integrated sensing and communication," *IEEE Commun. Surveys Tuts.*, vol. 24, no. 2, pp. 994–1034, 2nd Quart. 2022.
- [11] A. Ayyar and K. V. Mishra, "Robust communications-centric coexistence for Turbo-coded OFDM with non-traditional radar interference models," in *Proc. IEEE Radar Conference (RadarConf)*, pp. 1–6, 2019.
- [12] Y. Liu, Z. Wei, C. Yan, Z. Feng, and G. L. Stüber, "Effective capacity based power allocation for the coexistence of an integrated radar and communication system and a commercial communication system," *IEEE Access*, vol. 8, pp. 58629–58644, Mar. 2020.
- [13] L. Han, R. Liu, Z. Wang, Q. Liu, Q. Zhu, and J. S. Thompson, "Performance trade-off for integrated communication and data-assisted positioning in MIMO-OFDM system," *China Communications*, vol. 19, no. 11, pp. 129–147, Nov. 2022.
- [14] J. Sun, S. Ma, S. Li, R. Yang, M. Min, and G. Seco-Granados, "Robust beamforming for localization-aided millimeter wave communication systems," *IEEE Wireless Commun. Lett.*, vol. 11, no. 6, pp. 1278–1282, 2022.
- [15] G. Kwon, A. Conti, H. Park, and M. Z. Win, "Joint communication and localization in millimeter wave networks," *IEEE J. Sel. Topics Signal Process.*, vol. 15, no. 6, pp. 1439–1454, Nov. 2021.
- [16] Q. Wu and R. Zhang, "Intelligent reflecting surface enhanced wireless network via joint active and passive beamforming," *IEEE Trans. Wireless Commun.*, vol. 18, no. 11, pp. 5394–5409, Nov. 2019.
- [17] Q. Wu and R. Zhang, "Beamforming optimization for intelligent reflecting surface with discrete phase shifts," in *Proc. IEEE Int. Conf. Acoust., Speech, Signal Process. (ICASSP)*, pp. 7830–7833, May 2019.
- [18] C. Huang, A. Zappone, G. C. Alexandropoulos, M. Debbah, and C. Yuen, "Reconfigurable intelligent surfaces for energy efficiency in wireless communication," *IEEE Trans. Wireless Commun.*, vol. 18, no. 8, pp. 4157–4170, Aug. 2019.
- [19] Z. Abu-Shaban, K. Keykhosravi, M. F. Keskin, G. C. Alexandropoulos, G. Seco-Granados, and H. Wymeersch, "Near-field localization with a reconfigurable intelligent surface acting as lens," in *Proc. IEEE Int. Conf. Commun. (ICC)*, pp. 1–6, Aug. 2021.
- [20] A. Elzanaty, A. Guerra, F. Guidi, and M.-S. Alouini, "Reconfigurable intelligent surfaces for localization: Position and orientation error bounds," *IEEE Trans. Signal Process.*, vol. 69, pp. 5386–5402, Aug. 2021.
- [21] K. Keykhosravi, M. F. Keskin, G. Seco-Granados, P. Popovski, and H. Wymeersch, "RIS-enabled SISO localization under user mobility and spatial-wideband effects," *IEEE J. Sel. Topics Signal Process.*, vol. 16, no. 5, pp. 1125–1140, Aug. 2022.
- [22] Z. Yu, X. Hu, C. Liu, M. Peng, and C. Zhong, "Location sensing and beamforming design for IRS-enabled multi-user ISAC systems," *IEEE Trans. Signal Process.*, vol. 70, pp. 5178–5193, Nov. 2022.
- [23] H. Luo, R. Liu, M. Li, and Q. Liu, "RIS-aided integrated sensing and communication: Joint beamforming and reflection design," *IEEE Trans. Veh. Technol.*, Early Access, 2023, doi: 10.1109/TVT.2023.3248657.
- [24] X. Hu, C. Zhong, M.-S. Alouini, and Z. Zhang, "Robust design for IRS-aided communication systems with user location uncertainty," *IEEE Wireless Commun. Lett.*, vol. 10, no. 1, pp. 63–67, Jan. 2021.
- [25] J. He, H. Wymeersch, T. Sanguanpuak, O. Silven, and M. Juntti, "Adaptive beamforming design for mmWave RIS-aided joint localization and communication," in *Proc. IEEE Wireless Commun. Netw. Conf. Workshops (WCNCW)*, pp. 1–6, Apr. 2020.
- [26] M. Luan, B. Wang, Z. Chang, T. Hämäläinen, Z. Ling, and F. Hu, "Joint subcarrier and phase shifts optimization for RIS-aided localization-communication system," in *Proc. IEEE 95th Veh. Technol. Conf. (VTC-Spring)*, pp. 1–5, Jun. 2022.
- [27] S. Jeong, O. Simeone, and J. Kang, "Optimization of massive full-dimensional MIMO for positioning and communication," *IEEE Trans. Wireless Commun.*, vol. 17, no. 9, pp. 6205–6217, Sep. 2018.

- [28] S. Jeong, O. Simeone, A. Haimovich, and J. Kang, "Beamforming design for joint localization and data transmission in distributed antenna system," *IEEE Trans. Veh. Technol.*, vol. 64, no. 1, pp. 62–76, Jan. 2015.
- [29] S. M. Kay, *Fundamentals of Signal Processing—Estimation Theory*, Englewood Cliffs, NJ, USA: Prentice-Hall, 1993.
- [30] A. Fascista, A. Coluccia, H. Wymeersch, and G. Seco-Granados, "Millimeter-wave downlink positioning with a single-antenna receiver," *IEEE Trans. Wireless Commun.*, vol. 18, no. 9, pp. 4479–4490, Sep. 2019.
- [31] Y. Shen and M. Z. Win, "Fundamental limits of wideband localization — Part I: A general framework," *IEEE Trans. Inf. Theory*, vol. 56, no. 10, pp. 4956–4980, Oct. 2010.
- [32] Z. Abu-Shaban, H. Wymeersch, T. Abhayapala, and G. Seco-Granados, "Single-anchor two-way localization bounds for 5G mmWave systems," *IEEE Trans. Veh. Technol.*, vol. 69, no. 6, pp. 6388–6400, Jun. 2020.
- [33] Y. Shen and M. Z. Win, "Effect of path-overlap on localization accuracy in dense multipath environments," in *Proc. IEEE Int. Conf. Commun. (ICC)*, pp. 4197–4202, May 2008.
- [34] E. Leitinger, P. Meissner, C. Rüdiger, G. Dumphart, and K. Witrisal, "Evaluation of position-related information in multipath components for indoor positioning," *IEEE J. Sel. Areas Commun.*, vol. 33, no. 11, pp. 2313–2328, Nov. 2015.
- [35] S. Ma, Y. Zhang, H. Li, J. Sun, J. Shi, H. Zhang, C. Shen, and S. Li, "Covert beamforming design for intelligent-reflecting-surface-assisted IoT networks," *IEEE Internet Thing J.*, vol. 9, no. 7, pp. 5489–5501, Apr. 2022.
- [36] M. Grant and S. Boyd, "CVX: Matlab software for disciplined convex programming, version 2.1," [Online]. Available: <http://cvxr.com/cvx>, Mar. 2014.
- [37] Z. Q. Luo, W. K. Ma, A. M. C. So, Y. Ye, and S. Zhang, "Semidefinite relaxation of quadratic optimization problems," *IEEE Signal Process. Mag.*, vol. 27, no. 3, pp. 20–34, May 2010.
- [38] M. Bengtsson and B. Ottersten, "Optimal and suboptimal transmit beamforming," *handbook of antennas in wireless communications*, 2001.
- [39] Y. Shen, W. Dai, and M. Z. Win, "Optimal power allocation for active and passive localization," in *Proc. IEEE Global Commun. Conf. (GLOBECOM)*, pp. 3713–3718, Dec. 2012.
- [40] P. Liu, Y. Li, W. Cheng, X. Gao, and X. Huang, "Intelligent reflecting surface aided NOMA for millimeter-wave massive MIMO with lens antenna array," *IEEE Trans. Veh. Technol.*, vol. 70, no. 5, pp. 4419–4434, May 2021.
- [41] Z. Wei, L. Zhao, J. Guo, D. W. K. Ng, and J. Yuan, "Multi-beam NOMA for hybrid mmWave systems," *IEEE Trans. Commun.*, vol. 67, no. 2, pp. 1705–1719, Feb. 2019.
- [42] Z. Abu-Shaban, X. Zhou, T. Abhayapala, G. Seco-Granados, and H. Wymeersch, "Error bounds for uplink and downlink 3D localization in 5G millimeter wave systems," *IEEE Trans. Wireless Commun.*, vol. 17, no. 8, pp. 4939–4954, Aug. 2018.